Original Article

Tripling the detection view of high-frequency linear-array-based photoacoustic computed tomography by using two planar acoustic reflectors

Guo Li, Jun Xia, Kun Wang, Konstantin Maslov, Mark A. Anastasio, Lihong V. Wang

Department of Biomedical Engineering, Washington University in St. Louis, One Brookings Drive, St. Louis, MO 63130, USA

Correspondence to: Lihong V. Wang. Department of Biomedical Engineering, Washington University in St. Louis, One Brookings Drive, St. Louis, MO 63130, USA. Email: LHWANG@WUSTL.EDU.

Background: Linear-array-based photoacoustic computed tomography (PACT) suffers from a limited view. Circular scanning does increase the detection view angle but is time-consuming. Therefore, it is desirable to increase the detection view angle of linear-array-based PACT without sacrificing imaging speed.

Methods: Two planar acoustic reflectors placed at 120 degrees to each other were added to a linear-array-based PACT system. Each reflector redirects originally undetectable photoacoustic waves back to the transducer array elements, and together they triple the original detection view angle of the PACT system.

Results: Adding two reflectors increased the detection view angle from 80 to 240 degrees. As a comparison, a single-reflector PACT has a detection view angle of only 160 degrees. A leaf skeleton phantom with a rich vascular network was imaged with the double-reflector PACT, and most of its features were recovered.

Conclusions: The two acoustic reflectors triple the detection view angle of a linear-array-based PACT without compromising the original imaging speed. This nearly full-view detection capability produces higher-quality images than single-reflector PACT or conventional PACT without reflectors.

Keywords: Photoacoustic computed tomography (PACT); linear transducer array; limited view; view angle; acoustic reflector

Submitted Sep 02, 2014. Accepted for publication Oct 19, 2014.
doi: 10.3978/j.issn.2223-4292.2014.11.09
View this article at: http://dx.doi.org/10.3978/j.issn.2223-4292.2014.11.09

Introduction

Photoacoustic tomography (PAT) forms images by detecting photoacoustic waves originating from thermal expansion caused by pulsed light absorption in biological tissues. Because acoustic scattering is several orders of magnitude less than optical scattering in biological tissue, PAT can acquire images of optical absorption at a depth beyond the optical diffusion limit, while still maintaining high spatial resolution, defined by the ultrasonic detection (1). Photoacoustic computed tomography (PACT) is one implementation of PAT, where signals acquired from multiple detection positions are combined to reconstruct an image of the object (2). To accelerate data acquisition, PACT usually uses a transducer array with hundreds of elements. So far, linear transducer arrays (3-5), circular transducer arrays (6-8) and arc transducer arrays (9) have all been used in PACT. Although circular transducer arrays can achieve full-view image quality, they are expensively custom-made, and their central frequencies are relatively low (less than 10 MHz) due to manufacturing constraints, which limit the spatial resolution for small-object imaging. In contrast, linear transducer arrays are commonly used in ultrasonography. In particular, linear transducer arrays with high frequencies (central frequency >10 MHz) can be used to build high-resolution PACT. Moreover, linear transducer

arrays can also be easily integrated with ultrasound imaging systems, leading to co-registered photoacoustic-ultrasonic imaging, which provides both optical and ultrasonic contrasts (4,5,10).

However, linear-array-based PACT suffers from limited view. Due to the limited detection aperture of the whole array and the limited receiving angle of each element, linear transducer arrays cannot capture photoacoustic (PA) waves over a full 360 degrees in a two-dimensional (2D) image plane. In fact, only boundaries that are nearly perpendicular to the acoustic axis of the linear transducer array can be detected. To increase the detection view for linear-array-based PACT, several methods have been developed. The most straightforward and easiest way is to circularly or semi-circularly scan either the linear transducer array or the imaging sample (11-13). The time-consuming scan offsets the speed advantage of using a transducer array. Gateau *et al*. (14) proposed to use a ground glass diffuser to generate optical speckles as the illumination source, and by scanning the diffuser, they achieved full-view PACT images. However, this dynamic speckle method can image only shallow structures, and it still needs mechanical scanning. While an advanced algorithm (15) may be used to improve the imaging quality by removing streaking artifacts caused by the limited view, it cannot recover out-of-view boundaries. Ideally, we would like to enlarge the detection view of linear-array-based PACT without any mechanical scanning, in other words, without sacrificing the imaging speed. Acoustic reflectors redirect otherwise undetectable PA waves to the transducer array and hence increase the detection aperture (16). Cox *et al*. (17) proposed to use two acoustic reflectors normal to the linear transducer array to get an infinitely wide virtual transducer array. However, they demonstrate this full-view imaging capability only by numerical simulations, where each transducer element is assumed to be able to receive PA waves from all directions. In reality, the limited receiving angle of each transducer element would deteriorate the theoretical predictions. Huang *et al*. (18) experimentally proved that the detection view can be doubled by using a single 45-degree acoustic reflector adjacent to a linear transducer array. However, as the transducer array acceptance angle is typically less than 90 degrees, the doubled detection view from a single acoustic reflector is still insufficient to image more complex features. We need to further improve the detection view of a linear-array-based PACT. Moreover, Huang *et al*. utilized a low-frequency (5 MHz) linear transducer array, which is applicable to relatively large objects.

Materials and methods

In this study, we propose a high-frequency linear-array-based PACT using two acoustic reflectors set at 120 degrees relative to each other. It is compared against a linear-array-based PACT both without and with a single 45-degree acoustic reflector, named "conventional PACT" and "single-reflector PACT", respectively.

Figure 1A shows a schematic of the conventional PACT, which can collect only PA waves propagating towards the transducer array. The acceptance angle of each element is limited by the angular spread function, which is usually less than 60 degrees for high-frequency linear transducer arrays because of the relatively large ratio of the element width to the acoustic wavelength. Therefore, in *Figure 1A* the horizontal boundary segments with detectable PA waves propagating along the $-x$ direction can be reconstructed well, while the vertical boundary segments with undetectable PA waves propagating along the $\pm y$ direction cannot be reconstructed. To broaden the detection view, a 45-degree planar acoustic reflector was used to recover the vertical boundaries (18) (*Figure 1B*). With the aid of the acoustic reflector, the PA waves propagating along the $-y$ direction are redirected to the $-x$ direction, and then received by the transducer array. While a single acoustic reflector can double the detection view, it is not enough to cover a full 360 degrees, even for large acceptance angle transducer elements. Naturally, one can add more reflectors to further extend the detection view and recover more boundaries. *Figure 1C* shows acoustic reflectors set at an included angle of 120 degrees. Each reflector functions individually by redirecting the originally undetectable PA waves back to the transducer array elements, and together they recover more boundary features than a single reflector. In theory, two reflectors may cause multiple acoustic reflections between them. However, we did not observe obvious artifacts caused by multiple reflections in experiments, possibly due to reflection loss and acoustic attenuation, which rendered the multiple reflected signals negligible.

Images were reconstructed by using a filtered back-projection (FBP) algorithm (19). Although it is not mathematically exact for the 2D triangular measurement geometry, the FBP algorithm can be employed to generate boundary-enhanced images that accurately reveal the internal structures of the object. In future studies, advanced iterative image reconstruction methods (20,21) can be employed with the reflector geometry to produce more quantitatively accurate images at the expense of image

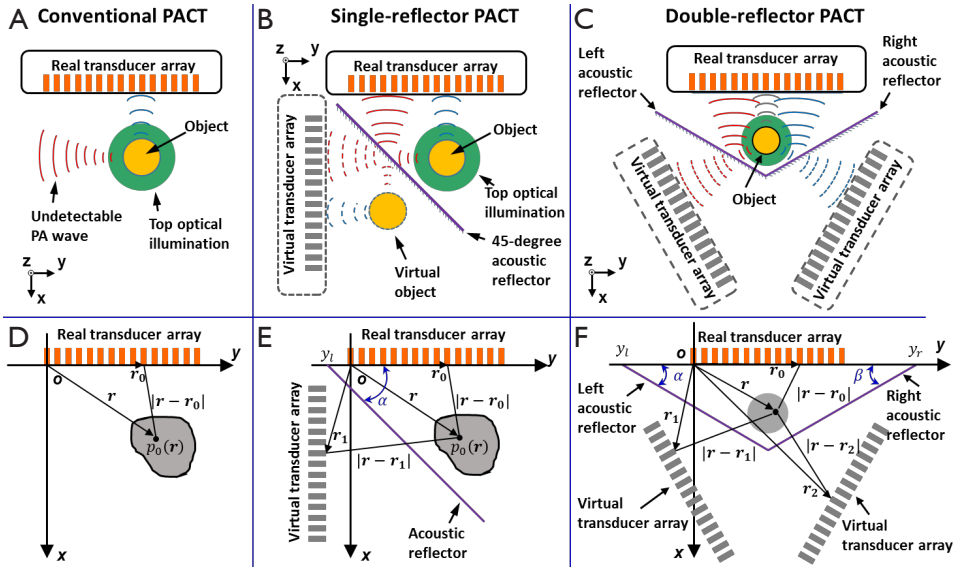

Figure 1 Schematics of the setups (A-C) and reconstruction processes (D-F) for conventional, single-reflector, and double-reflector linear-array-based PACT systems. $\boldsymbol{r}_0$, position of a real transducer element; $\boldsymbol{r}_1$ and $\boldsymbol{r}_2$, positions of virtual transducer elements; r, position inside the object; p_0, initial PA pressure. PACT, photoacoustic computed tomography.

reconstruction speed. The image reconstruction geometries for conventional, single-reflector, and double-reflector PACT are illustrated in *Figure 1D,E*, respectively. In contrast to the conventional PACT image reconstruction, where transducer array data are used only once, single-reflector PACT image reconstruction duplicates the data from the real transducer array to the mirrored virtual transducer array; the acoustic reflector is removed, and the filtered back projection is performed in a boundary-free infinite medium (16,18). The virtual transducer elements $\boldsymbol{r}_1$ (x_1,y_1) are mirrored from the real transducer elements $\boldsymbol{r}_0$ (x_0,y_0) about the acoustic reflection plane. The reconstruction of the double-reflector PACT is similar to that of a single-reflector PACT, except that there is a third transducer array that is mirrored from the real transducer array about the right reflector. Strictly speaking, the filtered back projection assumes a constant speed of sound (SOS) within the imaging field. However, the SOS may vary within the sample and between the sample and the coupling medium. These effects are not considered in this study, as it has been demonstrated that a small SOS variation only slightly degrades the image quality (22).

We experimentally tested the single-reflector PACT and double-reflector PACT using the aforementioned reconstruction algorithm. A 532 nm wavelength laser illuminated the target from the $-z$ to $+z$ direction (top illumination), as shown in *Figure 1*. The laser beam was generated from a second harmonic generator (OPOTEK Inc., Carlsbad, USA) pumped by a Nd:YAG laser (Brilliant, Quantel, Bozeman, USA) with 1064 nm output. This laser has a repetition rate of 20 Hz and an average pulse energy of 30 mJ. By using an engineering diffuser, the laser beam was expanded to a diameter of 1.6 cm on the top surface of the target, and therefore the laser fluence was 15 mJ/cm^2. A high-frequency linear transducer array with a central frequency of 15 MHz and a bandwidth of 9-18 MHz (MS200, Visualsonics Inc., Toronto, Canada) detected the PA waves. The MS200 linear transducer array has 256 elements, with a pitch of 125 μm and an effective detection aperture of 32.00 mm. The axial resolution (x-axis) in PACT was experimentally measured to be 113 μm, and the lateral resolution (y-axis) was 257 μm at a depth of 11 mm in water. The MS200 array also has a cylindrical acoustic lens with an elevational focal length of 18 mm and an elevational resolution of 1.2 mm in the elevational focal zone. The hypotenuse of an optical prism (PS911, Thorlabs Inc., Newton, USA) was used as the acoustic reflector for the single-reflector PACT. For double-reflector PACT, glass slides were used to reflect the PA waves. The prism and slides were made of BK7 glass, which has an acoustic impedance 10 times greater than that of the immersion liquid, and hence has a reflection coefficient close to unity. Although the amplitude and phase of the reflected acoustic wave change within the critical reflection angle of

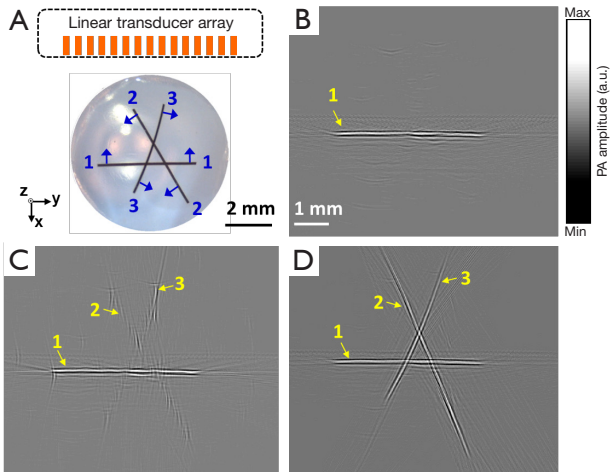

Figure 2 Simple phantom images. (A) Photograph of the crossed-hair phantom. PACT images acquired (B) without any acoustic reflector, (C) with one 45-degree planar acoustic reflector, and (D) with two ±120-degree planar acoustic reflectors. PACT, photoacoustic computed tomography.

26 degrees, here for simplicity we neglect this complexity and treat all reflections as total reflection without amplitude or phase change. As only a small amount of the signal comes from reflection within the critical angle, our assumption does not severely affect the structural image quality. In future quantitative studies, we will develop a more rigorous algorithm to account for this effect.

In our study, both the direct and reflected PA waves were detected by the MS200 transducer array, which was connected to a commercial PA imaging system (Vevo LAZR, Visualsonics Inc., Toronto, Canada). The 256 signal channels were multiplexed to a 64-channel data acquisition system, resulting in an imaging speed of 5 Hz. The raw channel data were then transferred to a PC where the FBP algorithm was applied to reconstruct PACT images.

Results

We first imaged a simple hair phantom as shown in *Figure 2A*. Three straight human hairs (labelled as "1-3") were embedded in a roughly triangular and planar arrangement in a 3% w/w agar gel. The generated PA waves propagated primarily along three directions at 120 degrees relative to each other, as indicated by blue arrows in *Figure 2A*. *Figure 2B* is the reconstructed PA image acquired by the conventional PACT. The horizontal hair labelled as "1" was recovered, but hairs 2 and 3 were missed due to the limited view. *Figure 2C* is the corresponding PA image acquired by the single-reflector PACT. While hair 1 was also reconstructed clearly, hairs 2 and 3 started to appear with obvious artifacts. *Figure 2D* shows the corresponding PA image acquired by the double-reflector PACT, where all three hairs were recovered clearly.

To quantitatively study the detection view enhancement, we imaged the cross-section of a tubular plastic drinking straw phantom in the *x-y* plane. The tube had an inner-diameter of 7.3 mm and a wall thickness of 0.15 mm. The circular tube generated PA waves in all 360 degrees in the 2D imaging plane, equivalent to the angular range from a point source at the center of the circle. Thereby we could quantitatively study the detection view of the three PACT systems. *Figure 3A* shows the PA image of the circular tube acquired by the conventional PACT, where the circle center was located at 11 mm away from the transducer surface. Both recovered top and bottom arcs have ~40 degrees of aperture with respect to the center, and this angle represents the receiving angle of the conventional PACT with respect to the circle center. Here the receiving angle is limited by two factors: the azimuth angle of the entire transducer aperture and the effective receiving angle of each individual transducer element. Because the azimuth aperture angle is ~55 degrees and the receiving angle of each transducer array element was experimentally measured to be ~40 degrees, the transducer element receiving angle is the limiting factor in this case. *Figure 3B* shows the reconstructed circular tube phantom imaged with the single-reflector PACT system. Compared with *Figure 3A*, there are two more arcs, so the detection view of the linear-array-based PACT has increased from 80 to 160 degrees, doubling the detection view of the conventional PACT system. *Figure 3C* shows the same circular tube phantom image acquired by the double-reflector PACT system. It is obvious that the detection view has been triply increased, from 80 to 240 degrees.

To verify the detection view enhancement, we imaged a complex phantom, a dehydrated leaf skeleton (*Figure 4A*). Compared with the hair phantom in *Figure 2A*, the leaf phantom has a rich vascular network and more complex features. *Figure 4B* shows a reconstructed image of the leaf phantom with the conventional PACT. Only boundaries close to the horizontal direction were recovered. *Figure 4C* shows an image of the phantom acquired by the single-reflector PACT. Some vertical boundaries were recovered, but there are still many unrecovered features. *Figure 4D* shows a double-reflector PACT image, which recovers most of the features identifiable in the photograph in *Figure 4A*.

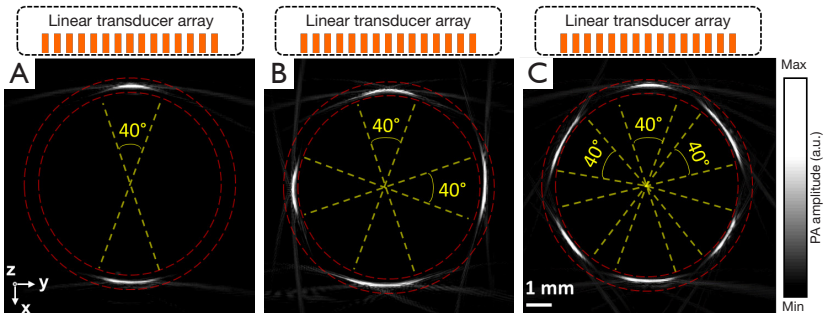

Figure 3 PACT images of a circular tube phantom acquired by (A) conventional PACT, (B) single-reflector PACT, and (C) double-reflector PACT. The view angle of the linear-array-based PACT doubles and triples with the single 45-degree planar acoustic reflector and two ±120-degree planar acoustic reflectors, respectively. PACT, photoacoustic computed tomography.

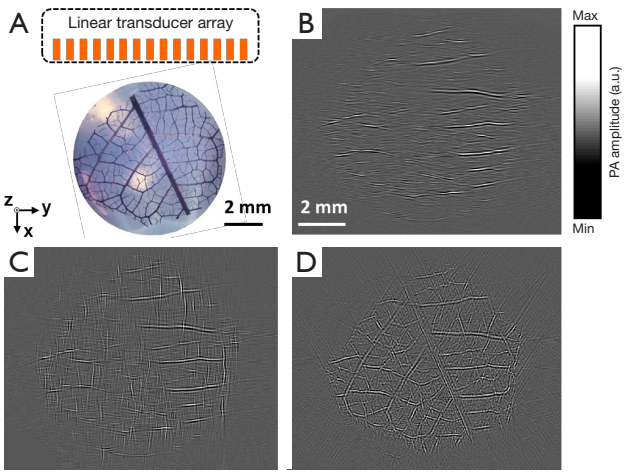

Figure 4 Leaf phantom images. (A) Photograph of the leaf phantom; (B) reconstructed PACT image without any acoustic reflector; (C) reconstructed PACT images with the 45-degree planar acoustic reflector; (D) reconstructed PACT images with two acoustic reflectors. PACT, photoacoustic computed tomography.

Discussion

This study proposed a linear-array-based double-reflector PACT and compared it with conventional PACT without any acoustic reflector and with single-reflector PACT. In comparison to the conventional PACT, double-reflector PACT triples the original detection view, while still keeping the original imaging speed. Although the double-reflector PACT still has not achieved 360-degree (i.e., full-view) detection due to the limited receiving angle of the single transducer element, it will be possible to achieve a full view in the future by using linear transducer arrays with larger element receiving angles and wider apertures.

Conclusions

By using two acoustic reflectors, we tripled the detection view angle of a linear-array-based PACT system, from 80 to 240 degrees, while maintaining the imaging speed. We introduced virtual transducer arrays into the image reconstruction plane to remove the boundaries created by reflectors, and then we applied the FBP algorithm for image reconstruction. Imaging a complex phantom demonstrated the enlarged detection view angle of the double-reflector method. Double-reflector reflector PACT may prove valuable in biomedical imaging studies where both high image quality and high imaging speed are desired.

Acknowledgements

The authors appreciate Prof. James Ballard's close reading of the manuscript. This work was sponsored by National Institute of Health (NIH) grants DP1 EB016986 (NIH Director's Pioneer Award), R01 CA186567 (NIH Director's Transformative Research Award), R01 EB016963, R01 CA159959 and S10 RR026922.

Disclosure: L.W. has a financial interest in Microphotoacoustics, Inc. and Endra, Inc., which, however, did not support this work. K.M. has a financial interest in Microphotoacoustics, Inc.

References

1. Wang LV. Multiscale photoacoustic microscopy and computed tomography. Nat Photonics 2009;3:503-9.
2. Wang LV, Hu S. Photoacoustic tomography: in vivo imaging from organelles to organs. Science

2012;335:1458-62.
3. Song L, Maslov K, Shung KK, Wang LV. Ultrasound-array-based real-time photoacoustic microscopy of human pulsatile dynamics in vivo. J Biomed Opt 2010;15:021303.
4. Kim C, Erpelding TN, Maslov K, Jankovic L, Akers WJ, Song L, Achilefu S, Margenthaler JA, Pashley MD, Wang LV. Handheld array-based photoacoustic probe for guiding needle biopsy of sentinel lymph nodes. J Biomed Opt 2010;15:046010.
5. Kim C, Erpelding TN, Jankovic L, Wang LV. Performance benchmarks of an array-based hand-held photoacoustic probe adapted from a clinical ultrasound system for non-invasive sentinel lymph node imaging. Philos Trans A Math Phys Eng Sci 2011;369:4644-50.
6. Gamelin J, Maurudis A, Aguirre A, Huang F, Guo P, Wang LV, Zhu Q. A real-time photoacoustic tomography system for small animals. Opt Express 2009;17:10489-98.
7. Xia J, Guo Z, Maslov K, Aguirre A, Zhu Q, Percival C, Wang LV. Three-dimensional photoacoustic tomography based on the focal-line concept. J Biomed Opt 2011;16:090505.
8. Xia J, Chatni MR, Maslov K, Guo Z, Wang K, Anastasio M, Wang LV. Whole-body ring-shaped confocal photoacoustic computed tomography of small animals in vivo. J Biomed Opt 2012;17:050506.
9. Brecht HP, Su R, Fronheiser M, Ermilov SA, Conjusteau A, Oraevsky AA. Whole-body three-dimensional optoacoustic tomography system for small animals. J Biomed Opt 2009;14:064007.
10. Yuan J, Xu G, Yu Y, Zhou Y, Carson PL, Wang X, Liu X. Real-time photoacoustic and ultrasound dual-modality imaging system facilitated with graphics processing unit and code parallel optimization. J Biomed Opt 2013;18:86001.
11. Yang DW, Xing D, Yang SH, Xiang LZ. Fast full-view photoacoustic imaging by combined scanning with a linear transducer array. Opt Express 2007;15:15566-75.
12. Kruger RA, Kiser WL Jr, Reinecke DR, Kruger GA. Thermoacoustic computed tomography using a conventional linear transducer array. Med Phys 2003;30:856-60.
13. Gateau J, Caballero MA, Dima A, Ntziachristos V. Three-dimensional optoacoustic tomography using a conventional ultrasound linear detector array: whole-body tomographic system for small animals. Med Phys 2013;40:013302.
14. Gateau J, Chaigne T, Katz O, Gigan S, Bossy E. Improving visibility in photoacoustic imaging using dynamic speckle illumination. Opt Lett 2013;38:5188-91.
15. Ma S, Yang S, Guo H. Limited-view photoacoustic imaging based on linear-array detection and filtered mean-backprojection-iterative reconstruction. J Appl Phys 2009;106:123104.
16. Wang LV, Yang X. Boundary conditions in photoacoustic tomography and image reconstruction. J Biomed Opt 2007;12:014027.
17. Cox BT, Arridge SR, Beard PC. Photoacoustic tomography with a limited-aperture planar sensor and a reverberant cavity. Inverse Problems 2007;23:S95.
18. Huang B, Xia J, Maslov K, Wang LV. Improving limited-view photoacoustic tomography with an acoustic reflector. J Biomed Opt 2013;18:110505.
19. Xu M, Wang LV. Universal back-projection algorithm for photoacoustic computed tomography. Phys Rev E Stat Nonlin Soft Matter Phys 2005;71:016706.
20. Huang C, Wang K, Nie L, Wang LV, Anastasio MA. Full-wave iterative image reconstruction in photoacoustic tomography with acoustically inhomogeneous media. IEEE Trans Med Imaging 2013;32:1097-110.
21. Zhang J, Anastasio MA, La Riviere PJ, Wang LV. Effects of different imaging models on least-squares image reconstruction accuracy in photoacoustic tomography. IEEE Trans Med Imaging 2009;28:1781-90.
22. Xia J, Huang C, Maslov K, Anastasio MA, Wang LV. Enhancement of photoacoustic tomography by ultrasonic computed tomography based on optical excitation of elements of a full-ring transducer array. Opt Lett 2013;38:3140-3.

Cite this article as: Li G, Xia J, Wang K, Maslov K, Anastasio MA, Wang LV. Tripling the detection view of high-frequency linear-array-based photoacoustic computed tomography by using two planar acoustic reflectors. Quant Imaging Med Surg 2015;5(1):57-62. doi: 10.3978/j.issn.2223-4292.2014.11.09

